A multi-year estimate of methane fluxes in Alaska from CARVE atmospheric observations

Scot M. Miller,[1] Charles E. Miller,[2] Roisin Commane,[3] Rachel Y.-W. Chang,[4] Steven J. Dinardo,[2] John M. Henderson,[5] Anna Karion,[6] Jakob Lindaas,[7] Joe R. Melton,[8] John B. Miller,[9] Colm Sweeney,[10] Steven C. Wofsy,[3] and Anna M. Michalak[1]

Corresponding author: Scot M. Miller, Department of Global Ecology, Carnegie Institution for Science, 260 Panama St., Stanford, CA 94305, USA. (scot.m.miller@gmail.com)

[1]Department of Global Ecology, Carnegie Institution for Science, Stanford, California, USA.

[2]Science Division, NASA Jet Propulsion Laboratory, Pasadena, California, USA.

[3]School of Engineering and Applied Sciences, Harvard University, Cambridge, MA, USA.

This article has been accepted for publication and undergone full peer review but has not been through the copyediting, typesetting, pagination and proofreading process, which may lead to differences between this version and the Version of Record. Please cite this article as doi: 10.1002/2016GB005419

Abstract.

Methane (CH_4) fluxes from Alaska and other arctic regions may be sensitive to thawing permafrost and future climate change, but estimates of both

[4]Department of Physics and Atmospheric Science, Dalhousie University, Halifax, Nova Scotia, Canada.

[5]Atmospheric and Environmental Research, Inc., Lexington, MA

[6]National Institute of Standards and Technology, Gaithersburg, Maryland, USA.

[7]Department of Atmospheric Science, Colorado State University, Fort Collins, Colorado, USA.

[8]Climate Research Division, Environment and Climate Change Canada, Victoria, Canada

[9]Global Monitoring Division, NOAA, Boulder, CO, USA.

[10]Cooperative Institute for Research in Environmental Sciences, University of Colorado, Boulder, Colorado, USA.

current and future fluxes from the region are uncertain. This study estimates CH_4 fluxes across Alaska for 2012 – 2014 using aircraft observations from the Carbon in Arctic Reservoirs Vulnerability Experiment (CARVE) and a geostatistical inverse model (GIM). We find that a simple flux model based on a daily soil temperature map and a static map of wetland extent reproduces the atmospheric CH_4 observations at the state-wide, multi-year scale more effectively than global-scale process-based models. This result points to a simple and effective way of representing CH_4 fluxes across Alaska. It further suggests that process-based models can improve their representation of key processes, and that more complex processes included in these models cannot be evaluated given the information content of available atmospheric CH_4 observations. In addition, we find that CH_4 emissions from the North Slope of Alaska account for 24% of the total statewide flux of 1.74 ± 0.26 Tg CH_4 (for May – Oct.). Global-scale process models only attribute an average of 3% of the total flux to this region. This mismatch occurs for two reasons: process models likely underestimate wetland extent in regions without visible surface water, and these models prematurely shut down CH_4 fluxes at soil temperatures near 0°C. Lastly, we find that the seasonality of CH_4 fluxes varied during 2012 – 2014, but that total emissions did not differ significantly among years, despite substantial differences in soil temperature and precipitation.

Key points:

- A simple model of soil temperature and wetland distribution can reproduce patterns in atmospheric CH_4 observations.
- The largest CH_4 fluxes in Alaska occur in lowland tundra – in the southwest (e.g., Yukon-Kuskokwim Delta) and North Slope.
- We do not find evidence for large year-to-year variability in total CH_4 fluxes from Alaska.

1. Introduction

Northern permafrost regions contain large quantities of soil organic carbon – up to 1300 Pg [*Hugelius et al.*, 2014]. This reservoir is equivalent to two times the amount of carbon currently in the atmosphere and 50% of all soil carbon in the world [*Tarnocai et al.*, 2009; *Hugelius et al.*, 2014]. Soil carbon can be converted to methane (CH_4) gas in wetlands and inundated soils via anaerobic respiration, and these wetlands are therefore an important component of the total global CH_4 budget. Estimates of global wetland fluxes or emissions range from 142 Tg to 285 Tg CH_4 per year, compared to total CH_4 emissions of 526 Tg to 852 Tg [*Kirschke et al.*, 2013]. CH_4 emissions from boreal and arctic wetlands account for 25 Tg to 100 Tg of this total [e.g., *McGuire et al.*, 2009; *Bousquet et al.*, 2011; *Melton et al.*, 2013; *Kirschke et al.*, 2013].

Climate warming in boreal and arctic regions will likely be twice the global mean [*Serreze and Barry*, 2011], and CH_4 fluxes could increase in the future due to these changes. Alaska is a particularly good case study, a location where these changes are acute. The rate of temperature change has recently accelerated in Alaska, and permafrost in the northern part of the state has warmed by 0.75° to 2.5°C since 1980 [*Markon et al.*, 2012]. In fact, a recent study suggests that ∼17% (13 Pg) of all soil carbon in Alaska could thaw by 2100 [*Mishra and Riley*, 2012]. These changes could bring about large-scale shifts in soil carbon dynamics across the state and concomitant changes in CH_4 fluxes [e.g., *Schuur et al.*, 2015].

CH_4 fluxes from high-latitude wetlands may play a critical role in global climate, but both current estimates and future projections of CH_4 fluxes from these regions are highly

uncertain, particularly for Alaska. A recent model comparison project found little agreement among CH_4 estimates for the state. Estimates of total emissions range from 0.8 to 6 Tg CH_4 yr^{-1} [*Melton et al.*, 2013; *Chang et al.*, 2014; *Fisher et al.*, 2014]. Future changes in wetland CH_4 fluxes are also uncertain; fluxes from high latitudes may increase anywhere from 6% to 35% per °C of global temperature increase [*Gedney et al.*, 2004; *Khvorostyanov et al.*, 2008; *O'Connor et al.*, 2010; *Koven et al.*, 2011; *Zhu et al.*, 2011]. Two recent global-scale inversions, by contrast, have not found any evidence for a trend in CH_4 fluxes from the arctic in 2000-2010 [*Bergamaschi et al.*, 2013; *Bruhwiler et al.*, 2014].

NASA's CARVE aircraft campaign provides unprecedented atmospheric greenhouse gas observations across the state of Alaska – observations that can be used to analyze current and infer future greenhouse gas fluxes from Alaska. The campaign collected observations during spring through fall of 2012 – 2015 across many heterogeneous ecosystems, including boreal taiga, subarctic tundra, and arctic tundra. These observations complement an existing, relatively sparse, long-term atmospheric observation network in Alaska: two NOAA global background sites (one on the North Slope and one in the Aleutian Islands) and a NOAA regular aircraft site near Fairbanks in the state's interior. A handful of previous studies have used CARVE, NOAA, and/or eddy flux data to estimate the magnitude [*Chang et al.*, 2014; *Karion et al.*, 2016a] and the seasonal cycle [*Karion et al.*, 2016a; *Zona et al.*, 2016] of Alaskan CH_4 fluxes. These studies found that the total CH_4 fluxes from Alaskan wetlands are much smaller than anthropogenic emissions sources in the continental US but are comparable in magnitude to other high-latitude wetlands like Canada's Hudson Bay Lowlands [*Chang et al.*, 2014; *Karion et al.*, 2016a]. In addition,

Zona et al. [2016] combined eddy flux data from the North Slope with CARVE observations and showed that 50% of fluxes occur during September – May, largely during times when soils are near but slightly above freezing.

The present study uses three years of CARVE aircraft and tower observations (2012 – 2014) and a geostatistical inverse model (GIM) to explore additional, key questions about CH_4 fluxes from Alaska. First, we analyze how CH_4 fluxes vary from one year to another. This analysis may indicate the sensitivity of CH_4 fluxes to year-to-year variability in environmental conditions. Second, we examine which environmental drivers best explain spatial and temporal patterns in the fluxes, as manifested in the atmospheric CH_4 measurements. These drivers can then be compared against the flux patterns in existing process-based models. Third, we analyze the spatial distribution of fluxes across the state. Alaska is topographically and ecologically heterogeneous, and we explore the relative contribution of its different physical and ecological environments to high-latitude CH_4 fluxes. Lastly, we compare our optimized CH_4 flux distribution to those estimated from process-based models and explore what these markedly different spatial patterns suggest for future biogeochemical modeling efforts.

2. Methods

2.1. CARVE aircraft and tower observations

The CARVE aircraft campaign sampled atmospheric greenhouse gas concentrations across the state during 2012 – 2015, and we utilize the first three years of observations in this study [*Budney et al.*, 2016]. The flight schedule varied by year, but flights usually occurred during May through October of each year and included 6 – 10 flight days each month. The campaign was based out of Fairbanks, Alaska, located in the state's eastern

interior region (65.815°N, 147.856°W). Flight lines repeatedly sampled southwest Alaska, the interior region, and Alaska's North Slope. Figure 1 shows the flight paths for June of each year. The flight patterns are relatively similar in other months. On any given flight, the aircraft usually spent significant time sampling within 150m of the surface but always executed at least one vertical profile to 3000 – 5000m during the course of the day to characterize the planetary boundary and residual layers.

Redundant Picarro analyzers measured CH_4, CO_2, and CO mole fractions continuously. The air sample for one instrument was dried prior to sampling, while the second analyzer measured ambient air and also reported water vapor concentrations. Post-calibrated differences in CH_4 derived from the two analyzers were less than 0.3 ppb CH_4 [*Chang et al.*, 2014]. Both analyzers measure CH_4 mole fractions every 2.5 s. We average this data horizontally into 5 km bins and vertically into 50 m bins below 1000 m above sea level (asl) and 100 m bins above 1000 m asl, as in *Chang et al.* [2014].

In addition to the CARVE aircraft observations, we also use hourly-averaged afternoon observations from the CARVE tower (NOAA site code CRV) [*Karion et al.*, 2016a, b]. The tower sits on a hilltop at 611 m asl in Fox, Alaska, approximately 20 km north of Fairbanks (64.986°N, 147.598°W). *Karion et al.* [2016a] provide a detailed discussion of the CRV tower observations.

2.2. Atmospheric modeling framework

We use the PWRF-STILT (Polar Weather Research and Forecasting - Stochastic Time-Inverted Lagrangian Transport) model, specifically developed for CARVE analysis, to relate surface CH_4 fluxes to atmospheric concentrations [*Chang et al.*, 2014; *Henderson et al.*, 2015; *Karion et al.*, 2016a; *Zona et al.*, 2016]. STILT is a particle back-trajectory

model [*Lin et al.*, 2003; *Gerbig et al.*, 2008]; it indicates where air masses travelled before reaching the observation location and time using PWRF meteorology. PWRF-STILT produces a footprint, a quantitative estimate of how surface fluxes in different upstream locations influence the observation site. For the setup here, each footprint has units of concentration per surface flux (ppb per μmol m^{-2} s^{-1}) on a 0.5° by 0.5° grid. The footprint can then be multiplied by an estimate of surface fluxes to model the effect of those fluxes (in ppb) at the observation site. Section S1, *Henderson et al.* [2015], and *Chang et al.* [2014] describe PWRF-STILT in greater detail. In addition, section S2 highlights several existing studies that have used PWRF-STILT and explores possible uncertainties in the PWRF-STILT simulations.

2.3. The geostatistical inverse model (GIM)

We estimate CH_4 fluxes in Alaska using a geostatistical inverse model (GIM) [e.g., *Kitanidis and Vomvoris*, 1983; *Michalak et al.*, 2004; *Gourdji et al.*, 2012; *Miller et al.*, 2014a]. We utilize a GIM because it requires fewer assumptions relative to other inverse modeling strategies. For example, a classical Bayesian inverse model requires a modeler to subjectively choose a bottom-up flux estimate and hard-code those flux patterns into the inversion prior. However, existing bottom-up estimates for Alaska show little agreement (sections 3.1 and 3.4). Instead, a GIM leverages auxiliary variables in place of a bottom-up estimate and objectively chooses these variables using atmospheric data. The auxiliary variables can consist of any spatial or temporal patterns that describe the fluxes, as manifested in the atmospheric observations. In our setup, the auxiliary variables include environmental drivers of CH_4 fluxes drawn from a meteorology model, land surface maps, and remote sensing. The inversion will scale the auxiliary data to minimize differences

with the atmospheric CH_4 observations. This component of the flux estimate is referred to as the "deterministic component" of the estimate. The GIM also estimates spatial and temporal patterns at grid scale – patterns that are implied by the atmospheric observations but that do not exist in the auxiliary variables. This component is referred to as the "stochastic component" of the flux estimate. The final flux estimate, referred to as the posterior estimate, is the sum of the deterministic and stochastic components:

$$\hat{\boldsymbol{s}} \;=\; \mathbf{X}\hat{\boldsymbol{\beta}} + \hat{\boldsymbol{\xi}} \tag{1}$$

In this equation, $\hat{\boldsymbol{s}}$ (dimensions $m \times 1$) is the posterior flux estimate, $\mathbf{X}$ ($m \times p$) is a matrix of p auxiliary variables defined at all grid locations and estimation times, $\hat{\boldsymbol{\beta}}$ ($p \times 1$) is the vector of estimated coefficients, and $\hat{\boldsymbol{\xi}}$ ($m \times 1$) is the estimated stochastic component. The GIM simultaneously estimates both the coefficients ($\hat{\boldsymbol{\beta}}$) and the stochastic component ($\hat{\boldsymbol{\xi}}$). Note that the coefficients ($\hat{\boldsymbol{\beta}}$) are constant in both space and time for the setup here. The stochastic component, by contrast, varies both spatially and temporally at model grid scale. Sections S3.1 and S3.2 list the full equations for the GIM and provide more detail on the specific setup used here.

To run the GIM, one must first decide which auxiliary variables to include in the deterministic model ($\mathbf{X}\boldsymbol{\beta}$). We use a model selection framework based upon the Bayesian Information Criterion to decide which auxiliary variables to includes within $\mathbf{X}$ [e.g., *Gourdji et al.*, 2012; *Miller et al.*, 2014a; *Shiga et al.*, 2014; *Fang and Michalak*, 2015; *Miller et al.*, 2016]. The model selection framework will score each possible linear combination of auxiliary variables based upon how well the model fits the atmospheric observations and upon the complexity of the model (see sections S3.3 for specific equations). The more complex a candidate model, the greater penalty it receives.

All model selection frameworks include a penalty for model complexity (e.g., partial F-test, Akaike information criterion, deviance information criterion, etc.), and this penalty ensures that the selected model is not an overfit to the data [e.g., *Zucchini*, 2000]. The inclusion of more auxiliary variables in the deterministic model will always improve model-data fit, and a model with n variables will always be able to perfectly reproduce a dataset of size n. Model selection uses a penalty to ensure that auxiliary variables are only included within a model if those variables substantially improve model-data fit.

We consider a number of potential auxiliary variables: the Kaplan wetland distribution estimate [*Bergamaschi et al.*, 2007; *Pickett-Heaps et al.*, 2011; *Miller et al.*, 2014a], the Kaplan soil carbon estimate [*Pickett-Heaps et al.*, 2011; *Miller et al.*, 2014a], maps of soil carbon content (30cm and 100cm) and peatland fractional coverage from NCSCD (the Northern Circumpolar Soil Carbon Database) [*Tarnocai et al.*, 2009; *Hugelius et al.*, 2014], soil inundation from *Matthews and Fung* [1987] and *Matthews* [1989], a map of lakes from the Global Lakes and Wetlands Database [*Lehner and Döll*, 2004], the EDGAR v4.2FT2010 anthropogenic emissions inventory [*Olivier and Janssens-Maenhout*, 2012], and the ASTER Global Digital Elevation Map [e.g., *Tachikawa et al.*, 2011]. These variables are static in time. We also consider a number of time-varying meteorological variables from the North American Regional Reanalysis (NARR) [*Mesinger et al.*, 2006]: soil temperature, an Arrhenius equation of soil temperature (see Eq. 1 in either *Pickett-Heaps et al.* [2011] or *Miller et al.* [2014a]), soil moisture, unfrozen soil moisture, moisture availability, specific humidity, relative humidity, snow depth, snow cover, and cloud cover. The Supplement describes the model selection framework in greater detail (section 3.3).

We estimate the fluxes at a daily temporal resolution for May – October of 2012 – 2014 and at a spatial resolution of 0.5° by 0.5° latitude-longitude. The geographic domain includes all of Alaska and portions of Canada and Siberia (160°E to 120°W longitude and 50°N to 75°N latitude, Figure 2). The resulting flux vector ($\boldsymbol{s}$) has $m = 1.94 \times 10^6$ elements. Furthermore, we use observations from the CARVE tower and aircraft observations up to 1500m agl. Observations above 1500m agl are usually in the free troposphere, and we do not use these observations in the GIM. We also remove individual observations when CO exceeds 150ppb, as in *Chang et al.* [2014]. This step removes obvious pollution or the influence of biomass burning plumes. The resulting observation vector contains 51500 elements (50090 from aircraft and 1410 from the tower).

3. Results & discussion

We first examine total CH_4 fluxes from Alaska and how those fluxes vary from year-to-year. We then explore the environmental datasets (i.e., auxiliary variables) that explain space-time patterns in the fluxes before discussing the spatial patterns of CH_4 fluxes in greater detail.

3.1. Total CH_4 fluxes from Alaska

We estimate a total Alaska CH_4 budget of 1.74 ± 0.26 Tg CH_4 for the months of May – Oct. (2012 – 2014 mean). Note that we do not quantify cold season CH_4 fluxes (Nov. – Apr.) in this study, and our CH_4 budget is lower than the unknown, annual total. In future efforts, year-round measurements would better capture the seasonal cycle and contribution of fluxes during the late fall through early spring.

Much of our estimated CH_4 fluxes are likely due to wetlands. We define wetland fluxes very broadly in this study as any flux related to the decomposition of organic matter. Section S4 discusses potential contributions of other emissions sources, including oil and gas extraction and marine fluxes.

Two existing top-down studies have estimated total CH_4 emissions for Alaska. *Karion et al.* [2016a] used data from the CARVE tower near Fairbanks, and *Chang et al.* [2014] used CARVE aircraft data. The former study quantified total CH_4 emissions ($\sim$1.5 Tg for May – Sept, 2012 – 2014) that are about 30% lower than the latter (2.1 $\pm$ 0.5 Tg for May – Sept. 2012). Neither estimate is significantly different from our estimate given the uncertainty bounds.

Relative to top-down studies, process-based CH_4 flux models estimate a large range of total budgets for Alaska [e.g., *Chang et al.*, 2014; *Fisher et al.*, 2014]. The recent WETCHIMP project compared seven global process-based models for the years 1993–2004 (Figure S5) [*Melton et al.*, 2013]. These models estimate a May–Oct CH_4 total of 0.65 Tg to 6.0 Tg CH_4 (multi-year mean). We compare these model estimates with one important caveat: the main strengths of these models may be their global to continental, not regional, magnitudes and distributions.

The total flux listed above (1.74 $\pm$ 0.26 Tg CH_4) represents our best estimate. We also explore the sensitivity of this estimate to different aspects of the GIM setup, including the boundary condition, covariance matrices, and auxiliary variables used in the GIM. To this end, we estimate the fluxes using an alternate boundary condition estimate and alternate altitude cutoff for the aircraft data (section 2.3). The total annual estimated

flux varied by less than 10% in each case. Section S7 describes these sensitivity tests in greater detail.

3.2. Year-to-year variability

We do not find evidence for large year-to-year variability in total CH_4 fluxes estimated for the 2012 – 2014 study period (Table 1). The variability among years is less than 10% of the total and is not statistically significant. This variability is less than that estimated by numerous process models. These models estimate a total CH_4 budget for peak years that is 33% to 88% higher than the lowest year, depending upon the model. The variability in May – Oct. 10 cm soil temperature during the WETCHIMP study period (1993-2004) is somewhat higher (1.8°C) than during the 2012 – 2014 time window of this study (1.0°C). With that said, year-to-year variability in the WETCHIMP models appears larger than the variability implied by the CARVE observations, and the sensitivity of the WETCHIMP fluxes to processes that vary on year-to-year time scales may be too large. In contrast to these process models, *Zona et al.* [2016] collected eddy flux measurements across the North Slope in 2013 and 2014 and found that total CH_4 fluxes were not significantly different between years.

Our results imply that year-to-year variability in temperature and precipitation may have a small effect on CH_4 fluxes relative to long term, structural changes in these ecosystems due to climate change. *Schuur et al.* [2015] explain that soil carbon decomposes at a rate of less than 1% per year under thawed, anaerobic conditions, and increases in wetland CH_4 fluxes due to climate change are likely to occur at the decadal, not year-to-year, scale.

Our total budget does not show any notable year-to-year variations, but the seasonal cycle of our estimate shows some variability among years (Figure 3). The peak summer estimate is highest in 2012 and lowest in 2014. Conversely, the fall and spring shoulder seasons have the largest fluxes in 2014. These year-to-year differences are not attributable to the temporal patterns in any environmental (i.e., auxiliary) dataset. Rather, these differences are the result of the stochastic component in the inversion, not the deterministic component, which varies by less than 3% among years. For example, the deterministic component includes NARR soil temperature (10 cm depth); NARR 10 cm soil temperature exhibits anomalies of up to $\pm 4^{\circ}$C at monthly time scales, but this variability is not large enough to cause large year-to-year changes in CH_4 fluxes estimated by the deterministic model (see section 3.3).

These year-to-year differences in the seasonality of fluxes (Figure 3) are likely caused by one (or more) of three factors. First, these differences could be driven by environmental conditions, conditions that are not mirrored in any of the auxiliary variables. During 2012, Alaska experienced a warm spring followed by a cool and wet summer, and warmer-than-average soil temperatures persist in NARR through the month of August. The combination of warm soils followed by high precipitation could explain the relatively large fluxes estimated for Jul.–Aug. 2012. By contrast, spring temperatures in 2013 were exceptionally cold with late thaw, followed by a warm and dry summer. Cool soil temperatures, however, persist in NARR 10 cm soil depth throughout much of the summer. These cold soil temperatures could explain why our estimated Jul.–Aug. fluxes in 2013 are lower than in 2012. During 2014, Alaska experienced a warm spring followed by a

cool and wet summer. These conditions could explain the relatively large springtime and low summertime fluxes in our estimate for 2014.

Second, these differences could reflect variations in sampling and advection patterns from one year to another. For example, poor weather prevented the CARVE aircraft from flying to the North Slope in a small number of months; the plane could not fly in conditions that required de-icing equipment and therefore could be biased toward good weather. In some months, the aircraft flew in the first half of the month, while in other months, the plane flew in the last half of the month. However, year-to-year differences in the seasonal cycle do not correlate with these differences in flight timing.

Third, these differences could reflect bias-type errors in the PWRF-STILT model that differ from one year to another. However, the error statistics of PWRF do not change substantially among seasons or years [*Henderson et al.*, 2015].

3.3. Environmental drivers of CH_4 fluxes

The model selection procedure determines which combination of environmental datasets best reproduces space-time patterns in CH_4 fluxes, as seen through the atmospheric observations. The best combination is a simple one: the Kaplan wetland map multiplied by an Arrhenius equation of 10 cm soil temperature from NARR. This combination of auxiliary variables provides the best balance between model-data fit and model simplicity.

The deterministic component estimated by the GIM has the following form:

$$\mathbf{X}\hat{\boldsymbol{\beta}} \;=\; 0.00268 + 322.2 f(\boldsymbol{T})\boldsymbol{K} \tag{2}$$

$$\text{where} \;\; f(T) \;=\; (\alpha 0.14 + 0.005(1-\alpha)) \exp\left(\frac{-309}{(T-227)}\right) \tag{3}$$

$$\text{and} \;\; \alpha \;=\; \min[\exp(T-303.15)/8, 1] \tag{4}$$

The deterministic component ($\mathbf{X}\hat{\boldsymbol{\beta}}$) has the same units as the posterior flux estimate (μmol m^{-2} s^{-1}), and Figure 4 displays the 2012 – 2014 mean. The deterministic component includes a modified Arrhenius equation of soil temperature (Eqs. 3 – 4), taken from *Pickett-Heaps et al.* [2011]. In these equations, T is NARR 10cm soil temperature in Kelvin, and α is an intermediate variable [refer to *Pickett-Heaps et al.*, 2011]. This Arrhenius equation ($f(T)$) fits the atmospheric observations better than using soil temperature directly as an auxiliary variable. In addition, the deterministic model includes a constant term, analogous to the intercept in a linear regression (section S3.3). Existing GIM studies always include a constant term within the deterministic model [e.g., *Gourdji et al.*, 2008, 2012; *Fang et al.*, 2014; *Fang and Michalak*, 2015].

The deterministic model is not a process-based flux model, but it represents a simple, effective way to describe space-time patterns in the fluxes using limited environmental information. The wetland map is static in time and drives the spatial distribution of fluxes while soil temperature is variable in time and drives the seasonal distribution of fluxes. Despite its simplicity, the space-time patterns in the deterministic model simulate the atmospheric observations reasonably well, with a correlation coefficient (r) of 0.55 and RMSE of 24.8 ppb (Figure 5). By comparison, the mean, observed CH_4 enhancement from CH_4 fluxes in Alaska is 22.5ppb.

In section S7, we also conduct several sensitivity tests using alternate combinations of auxiliary variables and explore how the auxiliary variables affect the CH_4 estimate. In these test cases, the deterministic model and final flux estimate become more spatially diffuse; these alternate combinations of auxiliary variables do not match the CARVE data

as well as the model in Eq. 2, and the GIM relies more heavily on the constant, intercept term than on the auxiliary variables.

A previous study by *Miller et al.* [2014a] applied model selection to evaluate CH_4 fluxes in boreal Canada and the Hudson Bay Lowlands and found a similar set of variables: the Kaplan wetland map multiplied by an Arrhenius equation of soil temperature from NARR (10 cm depth) and an estimate of unfrozen soil moisture from NARR. That study used CH_4 observations collected at towers across Canada and the northern US. This consistency bolsters our confidence in the results. It further points to a great need for accurate wetland maps and for accurate representation of soil temperature in process-based estimates.

A number of site-based studies from the North Slope further confirm the explanatory power of these environmental variables, albeit at a very different scale. For example, *Zona et al.* [2009] found that soil temperature explained 89% of variability in CH_4 fluxes inferred from eddy covariance measurements near Barrow, Alaska, and *Sturtevant et al.* [2012] found that soil inundation was the primary driver of seasonal patterns in chamber and eddy covariance measurements near Barrow. However, not all site-based studies agree on the role of different environmental drivers [e.g., *Sachs et al.*, 2008], and the studies above do not represent a uniform consensus in the literature.

The model selection framework does not choose any additional variables because no third variable describes enough additional variability to overcome the penalty for added model complexity. We find that the atmospheric observations are not sensitive to more detailed environmental processes (e.g., soil depth, moisture availability, etc.). If the atmospheric data were sensitive to more detailed processes or environmental variables, then those variables would have been chosen during the model selection process. Atmospheric

observations have limited ability to evaluate the impact of these additional variables on CH_4 fluxes; our results illustrate both the opportunities and limitations of intensive atmospheric measurement campaigns for evaluating surface CH_4 fluxes.

Despite its simplicity, the deterministic model describes flux patterns at regional, multi-year scales as well as process-based flux models. This result suggests that process-based models can significantly improve their CH_4 flux estimates by improving their treatment of key environmental parameters like soil temperature and wetland distribution. The individual WETCHIMP models yield correlation coefficients (r) that range from 0.54 to 0.32 and RMSEs that ranges from 25.9 to 60.5 ppb when compared against the atmospheric data (Figure 5). Those simulations cover 1993–2004, and we compare the multi-year means against the CARVE observations. The time period of these simulations is different from that of the present study, but it is unlikely that either the magnitude or spatial distribution of CH_4 fluxes across the state has changed dramatically in the intervening 10–15 years [e.g., *Schuur et al.*, 2015].

3.4. Spatial patterns in CH_4 fluxes

Our posterior flux estimate yields the largest fluxes in southwestern Alaska, the Seward Peninsula, and the North Slope (Figure 4a). The Yukon Delta National Wildlife Refuge and Yukon–Kuskokwim Delta of southwestern Alaska are a subarctic, lowland tundra with extensive wetlands, lakes, and rivers. The Seward Peninsula is covered by tundra and contains both lowland regions covered in wetlands and lakes as well as several small mountain chains less than 1,500m in height. The North Slope is an arctic, lowland tundra underlain with thick permafrost and many thermokarst features. All three regions have

few or no trees and generally saturated soils. In contrast to these areas, CH_4 fluxes are smaller in Alaska's boreal interior region.

The deterministic model captures many of these spatial features, including large CH_4 fluxes in southwestern Alaska and the North Slope. This comparison further confirms the capabilities of the deterministic model (Figure 4b). The stochastic component of the GIM includes additional variability in CH_4 fluxes, variability that does not map onto patterns in the deterministic model. The stochastic component removes fluxes from Alaska's interior and adds fluxes to the southwestern and North Slope regions (Figure 4c), regions that were regularly sampled by aircraft. These adjustments may hold several implications. First, wetland coverage may be higher in southwest Alaska and the North Slope and lower in the interior relative to the Kaplan estimate. Second, wetlands across the North Slope may be more productive (in terms of CH_4) relative to the temperature-driven patterns in the deterministic model [e.g., *Iwata et al.*, 2015; *Zona et al.*, 2016].

Our flux estimate for various regions of Alaska is also broadly consistent with available eddy flux data. *Zona et al.* [2016] measured CH_4 fluxes at five sites on the North Slope, and their measurements are comparable to the largest flux-producing regions of the North Slope in our estimate; they found peak summer fluxes of 2.4×10^{-2} μmol m^{-2} s^{-1} (multi-site mean) and a May – Oct. mean of $\sim 1 \times 10^{-2}$ μmol m^{-2} s^{-1}. In addition, *Iwata et al.* [2015] measured CH_4 fluxes in a black spruce forest near Fairbanks, and their results are comparable to the magnitude of our estimate across many parts of Alaska's interior. They measured fluxes that varied from from 0.09×10^{-2} – 0.2×10^{-2} μmol m^{-2} s^{-1} for the snow-free season, depending upon soil wetness at the given site.

We additionally compare the spatial distribution of our GIM estimate to the distribution of global, process-based estimates from the WETCHIMP project [*Melton et al.*, 2013]. Relative to those estimates, we find much higher fluxes across the North Slope (Figure 4d), a region that accounts for 24% (or 0.42 Tg CH_4) of the total CH_4 flux in our May–Oct. estimate compared to 3% (or 0.04 Tg CH_4), on average, in the WETCHIMP models (Figure 6a). The models show substantial disagreement across southwest region of the state, but all seven models estimate small fluxes for the North Slope (Figures 4e and S7).

Two factors explain the difference between our estimate and process-based estimates across the North Slope. First, process-based models estimate relatively low wetland coverage for the North Slope (Figure 6b). These models assign between 0.07% to 25% of the state's wetland area to the North Slope. The Kaplan wetland map, by contrast, assigns 39% of the state's wetland area to the North Slope, and this map is more consistent with atmospheric CH_4 observations than other wetland maps (see section 3.3). Most of the WETCHIMP models (five of the seven) use GIEMS to inform wetland area (see Figure 1 in *Melton et al.* [2013]). GIEMS is a remote sensing product that estimates surface inundation; it concentrates inundation in a small region near Barrow, a region with many surface lakes that are visible to satellites. The Kaplan map assigns wetlands more broadly across the North Slope in regions with and without substantial surface water.

Second, North Slope wetlands in the process models do not produce as much CH_4 as in our estimate (Figure 6c). In our estimate, one km^2 of wetlands on the North Slope produces about 75% as much CH_4 as one km^2 of wetlands in other, warmer regions of the state. This calculation is based on the Kaplan wetland distribution, and this calculated percentage could increase/decrease if the Kaplan estimate is too high/low across the North

Slope. In the process models, this number ranges from 10% to 43%. This difference in estimated productivity likely reflects missing temperature-related soil processes in process-based models. For example, SDGVM will not produce methane unless the monthly mean air temperature is greater than 5°C [*Wania et al.*, 2013], and air temperatures on the North Slope usually only exceed that threshold for zero to two months per year. Despite the high temperature threshold in SDGVM, it still reports higher North Slope CH_4 fluxes and higher productivity than several other process models (Figure 6a and 6c). These process models also contrast with recent eddy flux measurements on the North Slope by *Zona et al.* [2016], who found substantial CH_4 production from soils that are near freezing.

4. Conclusions

We estimate CH_4 fluxes in Alaska across multiple years (2012 – 2014) using observations from the recent CARVE airborne and tower campaigns and a geostatistical inverse model (GIM). This study focuses on the year-to-year variability, environmental drivers, and spatial distribution of CH_4 fluxes across the state.

We find little year-to-year variability in the fluxes across 2012, 2013, and 2014; total CH_4 fluxes for May – Oct. average 1.74 $\pm$ 0.26 Tg CH_4 and are within 10% from one year to another. This result contrasts with seven process-based estimates that vary between 33% to 88% among years [*Melton et al.*, 2013]. These results may indicate the sensitivity of CH_4 fluxes in Alaska to near-term variability in environmental conditions; even relatively large differences in temperature and precipitation among years did not translate into large differences in our CH_4 flux estimate. By contrast, process-based models may be too sensitive to variations in environmental drivers that occur on year-to-year time scales.

Our results further indicate that a small number of key environmental parameters can describe many spatial and temporal features in CH_4 fluxes from Alaska. This result provides a simple way to parameterize CH_4 fluxes at time scales comparable to the study period using only limited environmental information. This simple model of wetland area and soil temperature describes patterns in the fluxes more effectively than seven process-based estimates; these estimates could therefore improve the treatment of these key environmental drivers. This result cautions, however, that intensive, airborne observations from CARVE have limited ability to evaluate additional, more detailed processes in bottom-up flux models. Aircraft data represent the integrated signal of CH_4 fluxes over a large geographic area, and this study illustrates both the possibilities and limitations of this data for informing process-based estimates of greenhouse gas fluxes.

Lastly, our study reveals a number of broad spatial features in CH_4 fluxes. We find the largest fluxes in Alaska from lowland arctic and subarctic tundra. Many taiga regions in the interior are low in elevation but produce smaller fluxes. Our findings indicate large fluxes from the North Slope relative to seven process-based estimates. This difference is caused by two factors. First, process models appear to underestimate wetland area in regions of the North Slope without thermokarst lakes or obvious surface water. Second, these models shut down prematurely when sub-surface soils approach freezing temperatures. In contrast to these results for the North Slope, several recent studies indicate that process models overestimate CH_4 fluxes in warmer, boreal regions of North America [*Pickett-Heaps et al.*, 2011; *Miller et al.*, 2014a; *Wecht et al.*, 2014; *Miller et al.*, 2016]. Cold soil tundra is a larger contributor to North American CH_4 fluxes and warmer boreal regions a smaller contributor relative to process-based estimates. As a result, future

climate projections based upon these process models could underestimate CH_4-climate feedbacks for cold soil tundra and overestimate feedbacks in regions with warmer soils.

Acknowledgments. This work was supported by the Carnegie Distinguished Postdoctoral Fellowship. We thank Thomas Nehrkorn of Atmospheric and Environmental Research for his help with the PWRF-STILT model. Computing resources for this work were provided by the NASA High-End Computing (HEC) Program through the NASA Advanced Supercomputing (NAS) Division at Ames Research Center. Reanalysis data provided by the NOAA/OAR/ESRL PSD, Boulder, Colorado, USA, from their web site at http://www.esrl.noaa.gov/psd/. The CARVE data used in this study are available at http://dx.doi.org/10.3334/ORNLDAAC/1402 and https://ilma.jpl.nasa.gov/portal/browse/.

References

Becker, S. (2015), L-BFGS-B, converted from Fortran to C, with Matlab wrapper. `https://github.com/stephenbeckr/L-BFGS-B-C`. Last accessed 28 March, 2016.

Bergamaschi, P., et al. (2013), Atmospheric CH_4 in the first decade of the 21st century: Inverse modeling analysis using SCIAMACHY satellite retrievals and NOAA surface measurements, *J. Geophys. Res.: Atmos.*, *118*(13), 7350–7369, doi:10.1002/jgrd.50480.

Bergamaschi, P., et al. (2007), Satellite chartography of atmospheric methane from SCIAMACHY on board ENVISAT: 2. Evaluation based on inverse model simulations, *J. Geophys. Res.: Atmos.*, *112*(D2), doi:10.1029/2006JD007268.

Bousquet, P., et al. (2011), Source attribution of the changes in atmospheric methane for 2006–2008, *Atmos. Chem. Phys.*, *11*(8), 3689–3700, doi:10.5194/acp-11-3689-2011.

Bruhwiler, L., E. Dlugokencky, K. Masarie, M. Ishizawa, A. Andrews, J. Miller, C. Sweeney, P. Tans, and D. Worthy (2014), CarbonTracker-CH_4: an assimilation system for estimating emissions of atmospheric methane, *Atmos. Chem. Phys.*, *14*(16), 8269–8293, doi:10.5194/acp-14-8269-2014.

Budney, J. W., et al. (2016), CARVE: L2 Merged Atmospheric CO2, CO, O3 and CH4 Concentrations, Alaska, 2012-2015, *ORNL DAAC*, Oak Ridge, Tennessee, USA, doi: 10.3334/ORNLDAAC/1402.

Byrd, R. H., P. Lu, J. Nocedal, and C. Zhu (1995), A limited memory algorithm for bound constrained optimization, *SIAM Journal on Scientific Computing*, *16*(5), 1190–1208, doi:10.1137/0916069.

Chang, R. Y.-W., et al. (2014), Methane emissions from Alaska in 2012 from CARVE airborne observations, *Proc. Natl. Acad. Sci. U.S.A.*, *111*(47), 16,694–16,699, doi:10.1073/pnas.1412953111.

Corbeil, R. R., and S. R. Searle (1976), Restricted maximum likelihood (REML) estimation of variance components in the mixed model, *Technometrics*, *18*(1), pp. 31–38.

Fang, Y., and A. M. Michalak (2015), Atmospheric observations inform CO_2 flux responses to enviroclimatic drivers, *Global Biogeochem. Cycles*, *29*(5), 555–566, doi: 10.1002/2014GB005034, 2014GB005034.

Fang, Y., A. M. Michalak, Y. P. Shiga, and V. Yadav (2014), Using atmospheric observations to evaluate the spatiotemporal variability of CO_2 fluxes simulated by terrestrial biospheric models, *Biogeosciences*, *11*(23), 6985–6997, doi:10.5194/bg-11-6985-2014.

Fisher, J. B., et al. (2014), Carbon cycle uncertainty in the Alaskan Arctic, *Biogeosciences*, *11*(15), 4271–4288, doi:10.5194/bg-11-4271-2014.

Gedney, N., P. Cox, and C. Huntingford (2004), Climate feedback from wetland methane emissions, *Geophys. Res. Lett.*, *31*(20), doi:{10.1029/2004GL020919}.

Gerbig, C., S. Körner, and J. C. Lin (2008), Vertical mixing in atmospheric tracer transport models: error characterization and propagation, *Atmos. Chem. Phys.*, *8*(3), 591–602, doi:10.5194/acp-8-591-2008.

Gourdji, S. M., et al. (2012), North American CO_2 exchange: inter-comparison of modeled estimates with results from a fine-scale atmospheric inversion, *Biogeosciences*, *9*(1), 457–475, doi:10.5194/bg-9-457-2012.

Gourdji, S. M., K. L. Mueller, K. Schaefer, and A. M. Michalak (2008), Global monthly averaged CO_2 fluxes recovered using a geostatistical inverse modeling approach: 2. Results including auxiliary environmental data, *J. Geophys. Res.: Atmos.*, *113*(D21), doi:{10.1029/2007JD009733}.

Hegarty, J., R. R. Draxler, A. F. Stein, J. Brioude, M. Mountain, J. Eluszkiewicz, T. Nehrkorn, F. Ngan, and A. Andrews (2013), Evaluation of Lagrangian particle dispersion models with measurements from controlled tracer releases, *J. Appl. Meteor. Climatol.*, *52*(12), 2623–2637, doi:10.1175/JAMC-D-13-0125.1.

Henderson, J. M., et al. (2015), Atmospheric transport simulations in support of the Carbon in Arctic Reservoirs Vulnerability Experiment (CARVE), *Atmos. Chem. Phys.*, *15*(8), 4093–4116, doi:10.5194/acp-15-4093-2015.

Hudman, R. C., et al. (2008), Biogenic versus anthropogenic sources of CO in the United States, *Geophys. Res. Lett.*, *35*(4), doi:10.1029/2007GL032393, l04801.

Hugelius, G., et al. (2014), Estimated stocks of circumpolar permafrost carbon with quantified uncertainty ranges and identified data gaps, *Biogeosciences*, *11*(23), 6573–6593,

doi:10.5194/bg-11-6573-2014.

Iwata, H., Y. Harazono, M. Ueyama, A. Sakabe, H. Nagano, Y. Kosugi, K. Takahashi, and Y. Kim (2015), Methane exchange in a poorly-drained black spruce forest over permafrost observed using the eddy covariance technique, *Agricultural and Forest Meteorology*, *214–215*, 157 – 168, doi:10.1016/j.agrformet.2015.08.252.

Juncher Jorgensen, C., K. M. Lund Johansen, A. Westergaard-Nielsen, and B. Elberling (2015), Net regional methane sink in High Arctic soils of northeast Greenland, *Nat. Geosci.*, *8*(1), 20–23, doi:10.1038/ngeo2305.

Karion, A., et al. (2016a), Investigating Alaskan methane and carbon dioxide fluxes using measurements from the CARVE tower, *Atmos. Chem. Phys.*, *16*(8), 5383–5398, doi:10.5194/acp-16-5383-2016.

Karion, A., et al. (2016b), CARVE: CH_4, CO_2, and CO atmospheric concentrations, CARVE Tower, Alaska, 2012-2014, ORNL DAAC, Oak Ridge, Tennessee, USA, doi:10.3334/ORNLDAAC/1316.

Kass, R., and A. Raftery (1995), Bayes factors, *J. Am. Stat. Assoc.*, *90*(430), 773–795, doi:10.2307/2291091.

Khvorostyanov, D. V., P. Ciais, G. Krinner, and S. A. Zimov (2008), Vulnerability of east Siberia's frozen carbon stores to future warming, *Geophys. Res. Lett.*, *35*(10), doi:10.1029/2008GL033639.

Kirschke, S., et al. (2013), Three decades of global methane sources and sinks, *Nat. Geosci.*, *6*(10), 813–823, doi:10.1038/ngeo1955.

Kitanidis, P. K., and R. W. Lane (1985), Maximum likelihood parameter estimation of hydrologic spatial processes by the Gauss-Newton method, *J. Hydrol.*, *79*(1–2), 53 –

71, doi:10.1016/0022-1694(85)90181-7.

Kitanidis, P. K., and E. G. Vomvoris (1983), A geostatistical approach to the inverse problem in groundwater modeling (steady state) and one-dimensional simulations, *Water Resour. Res.*, *19*(3), 677–690, doi:10.1029/WR019i003p00677.

Kort, E. A., et al. (2008), Emissions of CH_4 and N_2O over the United States and Canada based on a receptor-oriented modeling framework and COBRA-NA atmospheric observations, *Geophys. Res. Lett.*, *35*(18), doi:10.1029/2008gl034031.

Koven, C. D., B. Ringeval, P. Friedlingstein, P. Ciais, P. Cadule, D. Khvorostyanov, G. Krinner, and C. Tarnocai (2011), Permafrost carbon-climate feedbacks accelerate global warming, *Proc. Natl. Acad. Sci. U. S. A.*, *108*(36), 14,769–14,774, doi:10.1073/pnas.1103910108.

Lehner, B., and P. Döll (2004), Development and validation of a global database of lakes, reservoirs and wetlands, *J. Hydrol.*, *296*(1-4), 1 – 22, doi:10.1016/j.jhydrol.2004.03.028.

Lin, J., C. Gerbig, S. Wofsy, A. Andrews, B. Daube, K. Davis, and C. Grainger (2003), A near-field tool for simulating the upstream influence of atmospheric observations: The Stochastic Time-Inverted Lagrangian Transport (STILT) model, *J. Geophys. Res.: Atmos.*, *108*(D16), doi:10.1029/2002jd003161.

Markon, C. J., S. F. Trainor, and F. S. Chapin III (2012), The United States National Climate Assessment – Alaska technical regional report, *Circular 1379*, US Geological Survey. `http://pubs.usgs.gov/circ/1379/`. Last accessed 8 Jul 2016.

Matthews, E. (1989), Global data bases on distribution, characteristics and methane emission of natural wetlands: Documentation of archived data tape, *NASA TM-4153*, National Aeronautics and Space Administration, Washington, DC. `http://pubs.giss.`

nasa.gov/abs/ma08500r.html. Last accessed 8 Jul 2016.

Matthews, E., and I. Fung (1987), Methane emission from natural wetlands: Global distribution, area, and environmental characteristics of sources, *Global Biogeochem. Cycles*, *1*(1), 61–86, doi:10.1029/GB001i001p00061.

McGuire, A. D., et al. (2009), Sensitivity of the carbon cycle in the Arctic to climate change, *Ecol. Monogr.*, *79*(4), 523–555, doi:10.1890/08-2025.1.

Melton, J. R., et al. (2013), Present state of global wetland extent and wetland methane modelling: conclusions from a model inter-comparison project (WETCHIMP), *Biogeosciences*, *10*(2), 753–788, doi:10.5194/bg-10-753-2013.

Mesinger, F., et al. (2006), North American Regional Reanalysis., *Bull. Am. Meteorol. Soc.*, *87*, 343–360, doi:10.1175/BAMS-87-3-343.

Michalak, A., L. Bruhwiler, and P. Tans (2004), A geostatistical approach to surface flux estimation of atmospheric trace gases, *J. Geophys. Res.: Atmos.*, *109*(D14), doi:10.1029/2003JD004422.

Miller, S. M., et al. (2008), Sources of carbon monoxide and formaldehyde in North America determined from high-resolution atmospheric data, *Atmos. Chem. Phys.*, *8*(24), 7673–7696, doi:10.5194/acp-8-7673-2008.

Miller, S. M., et al. (2013), Anthropogenic emissions of methane in the United States, *Proc. Natl. Acad. Sci. U.S.A.*, *110*(50), 20,018–20,022, doi:10.1073/pnas.1314392110.

Miller, S. M., et al. (2014a), Observational constraints on the distribution, seasonality, and environmental predictors of North American boreal methane emissions, *Global Biogeochem. Cycles*, *28*(2), 146–160, doi:10.1002/2013GB004580.

Miller, S. M., A. M. Michalak, and P. J. Levi (2014b), Atmospheric inverse modeling with known physical bounds: an example from trace gas emissions, *Geosci. Model Dev.*, *7*(1), 303–315, doi:10.5194/gmd-7-303-2014.

Miller, S. M., et al. (2016), Evaluation of wetland methane emissions across North America using atmospheric data and inverse modeling, *Biogeosciences*, *13*(4), 1329–1339, doi:10.5194/bg-13-1329-2016.

Mishra, U., and W. J. Riley (2012), Alaskan soil carbon stocks: spatial variability and dependence on environmental factors, *Biogeosciences*, *9*(9), 3637–3645, doi:10.5194/bg-9-3637-2012.

Nehrkorn, T., J. Eluszkiewicz, S. C. Wofsy, J. C. Lin, C. Gerbig, M. Longo, and S. Freitas (2010), Coupled Weather Research and Forecasting-Stochastic Time-Inverted Lagrangian Transport (WRF-STILT) model, *Meteorology and Atmospheric Physics*, *107*(1-2), 51–64, doi:10.1007/s00703-010-0068-x.

O'Connor, F. M., et al. (2010), Possible role of wetlands, permafrost, and methane hydrates in the methane cycle under future climate change: A review, *Rev. Geophys.*, *48*, doi:10.1029/2010RG000326.

Olivier, J., and G. Janssens-Maenhout (2012), *CO_2 emissions from fuel combustion, 2012 edition*, chap. III: Greenhouse-gas emissions, International Energy Agency, Paris.

Pickett-Heaps, C. A., et al. (2011), Magnitude and seasonality of wetland methane emissions from the Hudson Bay Lowlands (Canada), *Atmos. Chem. Phys.*, *11*(8), 3773–3779, doi:10.5194/acp-11-3773-2011.

Sachs, T., C. Wille, J. Boike, and L. Kutzbach (2008), Environmental controls on ecosystem-scale CH_4 emission from polygonal tundra in the Lena River Delta, Siberia,

J. Geophys. Res.: Biogeosci., *113*(G3), doi:10.1029/2007JG000505, g00A03.

Schuur, E. A. G., et al. (2015), Climate change and the permafrost carbon feedback, *Nature*, *520*(7546), 171–179, doi:10.1038/nature14338.

Serreze, M. C., and R. G. Barry (2011), Processes and impacts of Arctic amplification: A research synthesis, *Global and Planetary Change*, *77*(1 - 2), 85 – 96, doi:10.1016/j.gloplacha.2011.03.004.

Shakhova, N., I. Semiletov, A. Salyuk, V. Yusupov, D. Kosmach, and Ö. Gustafsson (2010), Extensive methane venting to the atmosphere from sediments of the East Siberian Arctic Shelf, *Science*, *327*(5970), 1246–1250, doi:10.1126/science.1182221.

Shiga, Y. P., A. M. Michalak, S. M. Gourdji, K. L. Mueller, and V. Yadav (2014), Detecting fossil fuel emissions patterns from subcontinental regions using North American in situ CO_2 measurements, *Geophys. Res. Lett.*, *41*(12), 4381–4388, doi:10.1002/2014GL059684, 2014GL059684.

Sturtevant, C. S., W. C. Oechel, D. Zona, Y. Kim, and C. E. Emerson (2012), Soil moisture control over autumn season methane flux, Arctic Coastal Plain of Alaska, *Biogeosciences*, *9*(4), 1423–1440, doi:10.5194/bg-9-1423-2012.

Tachikawa, T., et al. (2011), ASTER Global Digital Elevation Model Version 2 - summary of validation results. `http://pubs.er.usgs.gov/publication/70005960`. Last accessed 8 Jul 2016.

Tarnocai, C., J. G. Canadell, E. A. G. Schuur, P. Kuhry, G. Mazhitova, and S. Zimov (2009), Soil organic carbon pools in the northern circumpolar permafrost region, *Global Biogeochem. Cycles*, *23*, doi:10.1029/2008GB003327.

Turner, A. J., et al. (2015), Estimating global and North American methane emissions with high spatial resolution using GOSAT satellite data, *Atmos. Chem. Phys.*, *15*(12), 7049–7069, doi:10.5194/acp-15-7049-2015.

Walter, K. M., L. C. Smith, and F. Stuart Chapin (2007), Methane bubbling from northern lakes: present and future contributions to the global methane budget, *Philos. Trans. R. Soc., A*, *365*(1856), 1657–1676, doi:10.1098/rsta.2007.2036.

Walter Anthony, K. M., P. Anthony, G. Grosse, and J. Chanton (2012), Geologic methane seeps along boundaries of arctic permafrost thaw and melting glaciers, *Nat. Geosci.*, *5*(6), 419–426, doi:10.1038/ngeo1480.

Wania, R., et al. (2013), Present state of global wetland extent and wetland methane modelling: methodology of a model inter-comparison project (WETCHIMP), *Geosci. Model Dev.*, *6*(3), 617–641, doi:10.5194/gmd-6-617-2013.

Wecht, K. J., D. J. Jacob, C. Frankenberg, Z. Jiang, and D. R. Blake (2014), Mapping of North American methane emissions with high spatial resolution by inversion of SCIAMACHY satellite data, *J. Geophys. Res.: Atmos.*, *119*(12), 7741–7756, doi:10.1002/2014JD021551.

Wik, M., B. F. Thornton, D. Bastviken, J. Uhlbck, and P. M. Crill (2016), Biased sampling of methane release from northern lakes: A problem for extrapolation, *Geophys. Res. Lett.*, *43*(3), 1256–1262, doi:10.1002/2015GL066501, 2015GL066501.

Yadav, V., and A. M. Michalak (2013), Improving computational efficiency in large linear inverse problems: an example from carbon dioxide flux estimation, *Geosci. Model Dev.*, *6*(3), 583–590, doi:10.5194/gmd-6-583-2013.

Zhu, X., Q. Zhuang, M. Chen, A. Sirin, J. Melillo, D. Kicklighter, A. Sokolov, and L. Song (2011), Rising methane emissions in response to climate change in Northern Eurasia during the 21st century, *Environ. Res. Lett.*, *6*(4), 045211, doi:10.1088/1748-9326/6/4/045211.

Zona, D., W. C. Oechel, J. Kochendorfer, K. T. Paw U, A. N. Salyuk, P. C. Olivas, S. F. Oberbauer, and D. A. Lipson (2009), Methane fluxes during the initiation of a large-scale water table manipulation experiment in the Alaskan Arctic tundra, *Global Biogeochem. Cycles*, *23*(2), doi:10.1029/2009GB003487, gB2013.

Zona, D., et al. (2016), Cold season emissions dominate the arctic tundra methane budget, *Proc. Natl. Acad. Sci. U.S.A.*, *113*(1), 40–45, doi:10.1073/pnas.1516017113.

Zucchini, W. (2000), An introduction to model selection, *Journal of Mathematical Psychology*, *44*(1), 41 – 61, doi:10.1006/jmps.1999.1276.

Table 1. Methane emissions for Alaska (May - Oct)

Year	Emissions (Tg CH_4)
2012	1.80 ± 0.45
2013	1.65 ± 0.43
2014	1.77 ± 0.45
Mean	1.74 ± 0.26

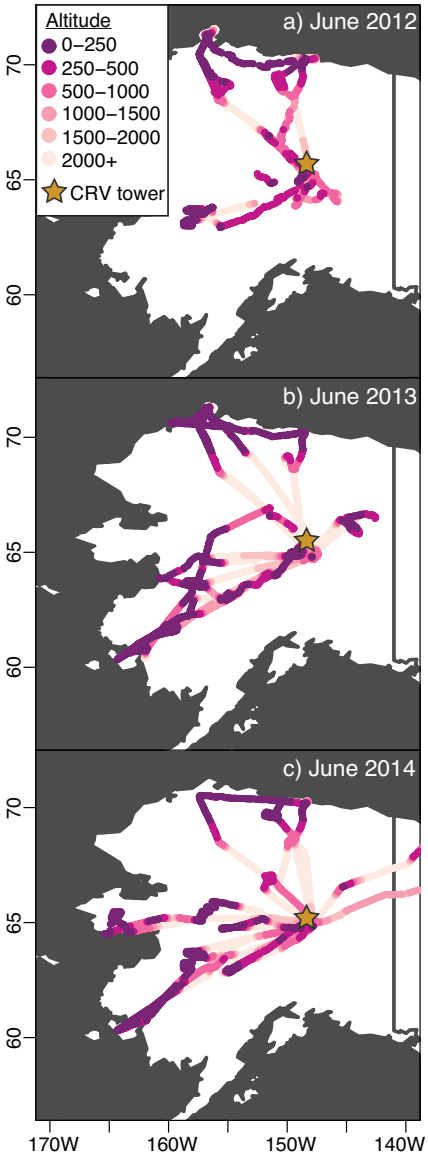

Figure 1. Maps of CARVE aircraft flights for June of each year. The flight paths are color-coded by altitude (in meters).

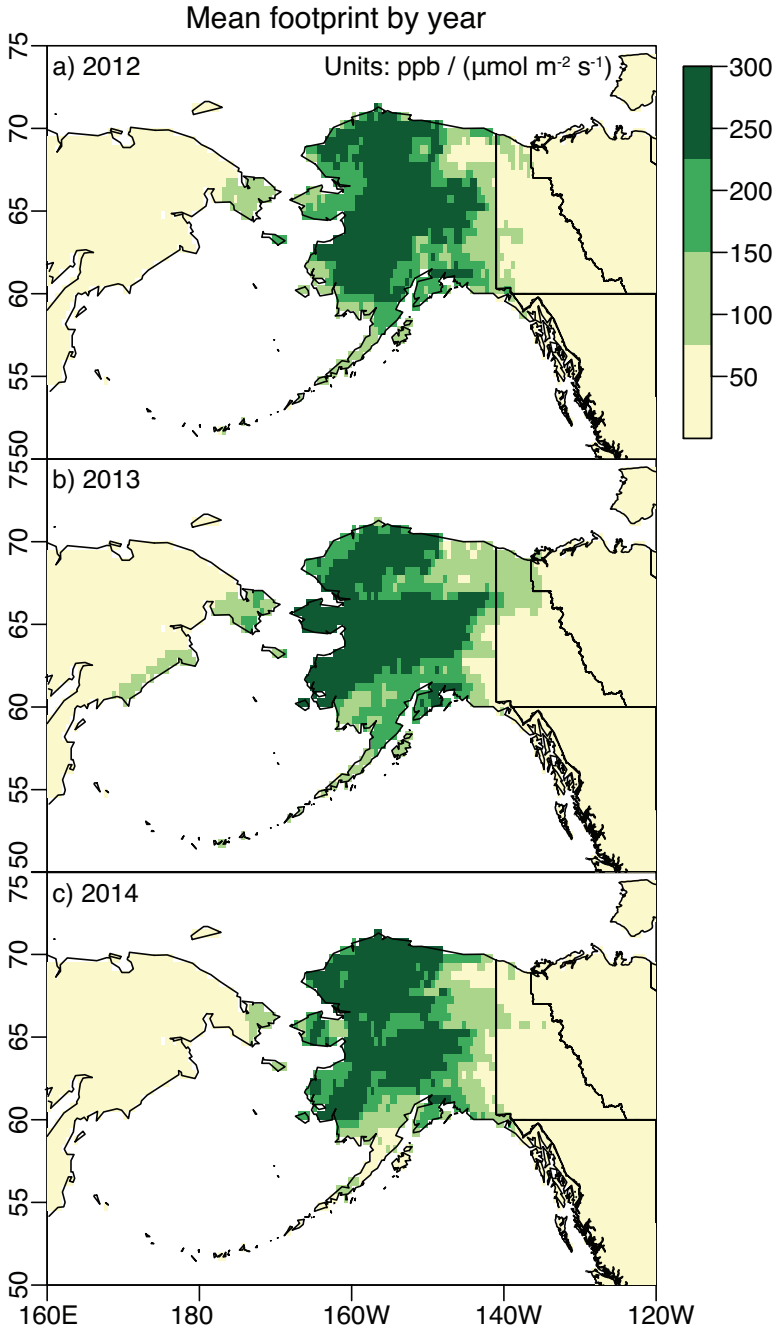

Figure 2. Panels visualize the annually-averaged PWRF-STILT observation sensitivity or footprint (aircraft and tower) for (a) 2012, (b) 2013, and (c) 2014. This figure displays the entire geographic domain used in the geostatitical inverse model (GIM). The sensitivities are highest over Alaska and minimal over Canada and Siberia. As such, we only report estimated CH_4 fluxes for Alaska.

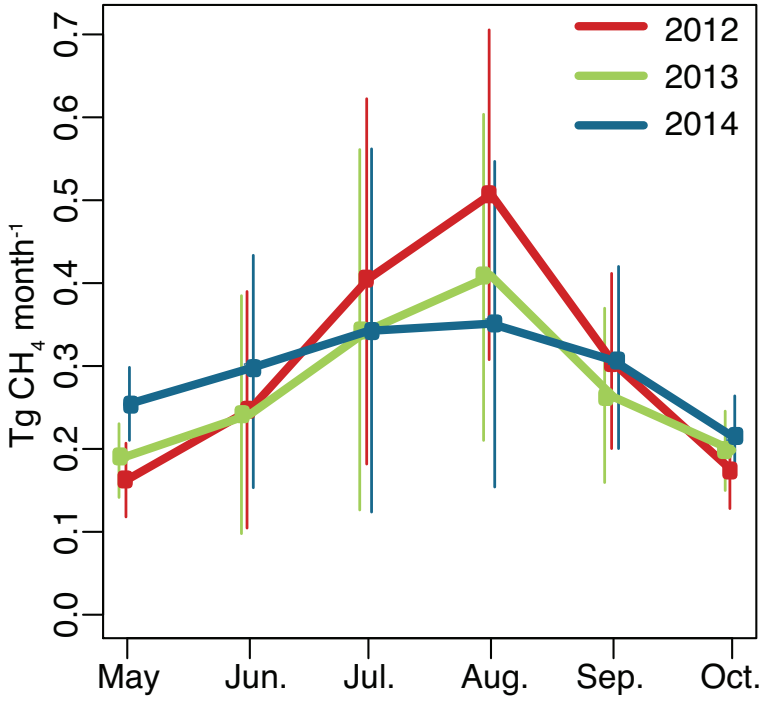

Figure 3. Estimated CH_4 budgets for Alaska by month for 2012 – 2014. The vertical lines show the associated uncertainties (one standard deviation).

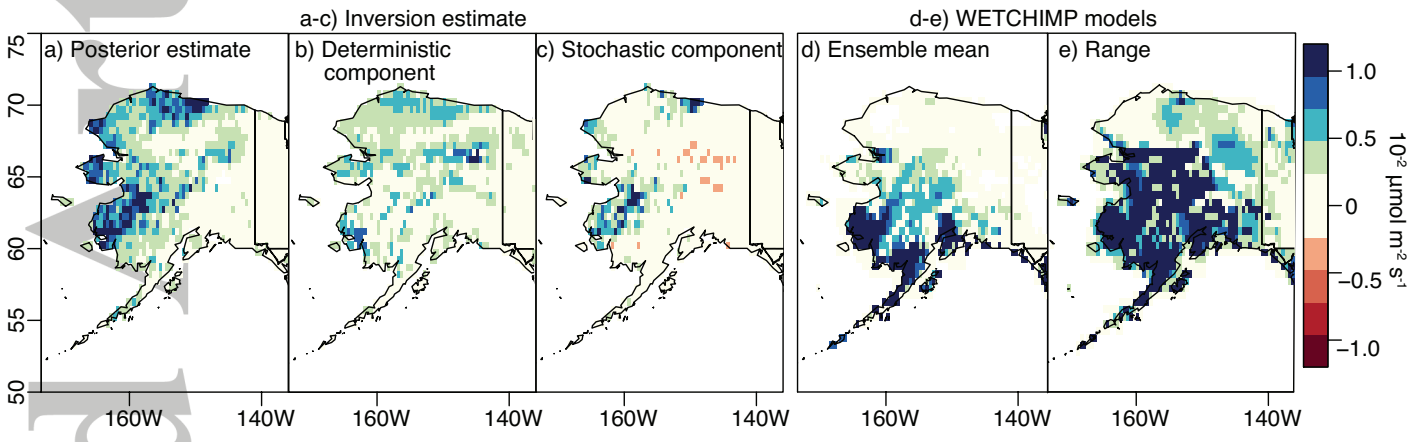

Figure 4. Panel (a) displays the CH_4 fluxes estimated by the GIM, averaged over all time periods (May – Oct., 2012 – 2014). Panels (b) and (c) illustrate the individual components of the posterior flux estimate; the sum of these two panels equals the posterior estimate in panel (a). Panels (d) and (e) display the mean and range, respectively, of seven process-based CH_4 fluxes estimates from the recent WETCHIMP model comparison project [*Melton et al.*, 2013].

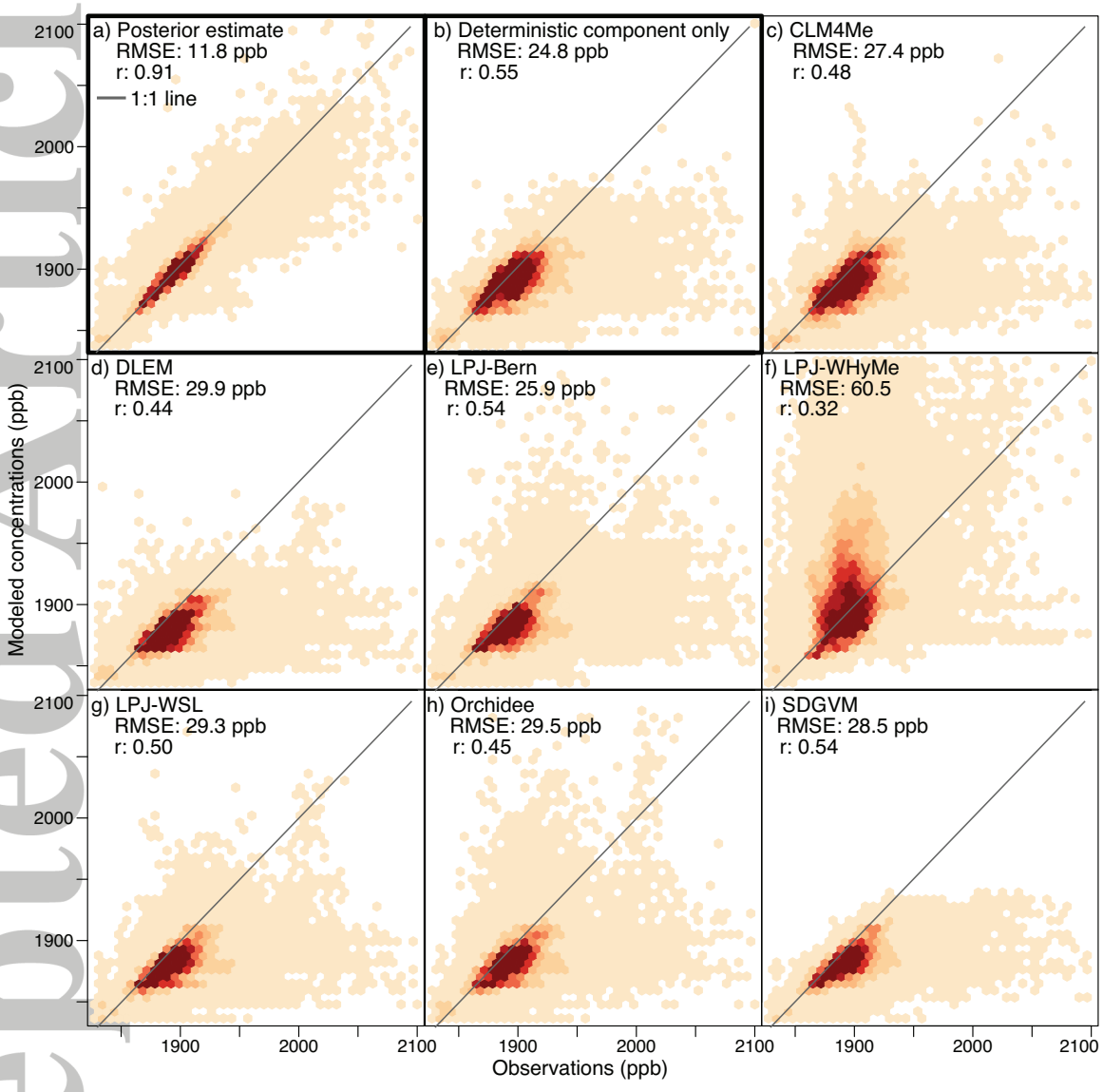

Figure 5. This plot compares atmospheric CH_4 concentrations modeled with PWRF-STILT against CH_4 observations from the CARVE aircraft and CRV tower. We model CH_4 concentrations using a number of flux estimates: (a) the posterior estimate from the GIM, (b) the deterministic component from the GIM, and (c-i) process-based flux estimates from the WETCHIMP comparison study [*Melton et al.*, 2013]. Darker colors indicate a higher density of points in each scatter plot. Note that the process-based estimates are more comparable to the deterministic model than the posterior estimate; the process-based estimates and deterministic model rely on auxiliary variables or environmental driver datasets. In contrast, the posterior estimate also includes fluxes that do not map on to any auxiliary variable.

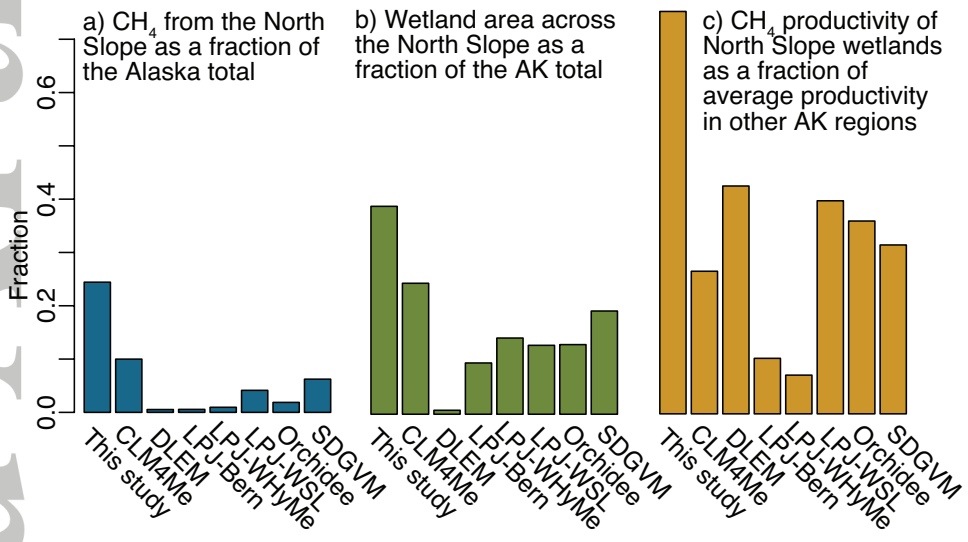

Figure 6. The individual panels (a–c) of this figure display CH_4 fluxes, wetland area, and CH_4 productivity (i.e., CH_4 fluxes per unit of wetland area) relative to the entire state of Alaska. Process-based models estimate relatively small fluxes for the North Slope (panel a). This result has two causes: process-based models estimate relatively low wetland area for the N. Slope (panel b) and low relative CH_4 productivity for that region (panel c). Note that this figure uses annual maximum wetland extent. Some, but not all, models also report wetland area at the monthly scale.